SUPPLEMENTARY INFORMATION

Coupling of Spin and Orbital Motion of Electrons in Carbon Nanotubes

F. Kuemmeth*, S. Ilani*, D. C. Ralph and P. L. McEuen

Laboratory of Atomic and Solid State Physics, Department of Physics, Cornell University, Ithaca NY 14853

1. Identification of the first electron and the first hole

In this paper we measure the energy spectrum of a single charge carrier, an electron or a hole, in a nanotube (NT) quantum dot (QD). Having a single carrier is central to our experiment as it allows us to avoid electronic interactions between carriers and to unambiguously identify the effects of spin-orbit interactions. Here we explain in more detail how we determine that there is a single carrier in the dot.

We start by identifying the transition from electrons to holes in the addition spectrum with the Coulomb valley labeled "0" in figure 1e, based on two observations: First, this valley is significantly larger than all other valleys, reflecting the added contribution of the bandgap to the addition energy (quantitative analysis below). Second, electrons and holes can be distinguished by their response to magnetic field (Fig. 3a). At large fields, such that the orbital coupling dominates over the level spacing in the dot, electrons and holes rotate in opposite directions around the NT circumference. This leads to opposite signs of $dV_g / dB_{\|}$ for electrons and holes (figure 3a, $B_{\|}$>200 mT). Note that this also means that the energy gap decreases with increasing magnetic field. To confirm that the first Coulomb valleys on the electron and hole sides correspond to the first electron and first hole in the dot it is enough to show that we observe all the charge states in the transport measurements and that there are no non-conducting charge states within the 0^{th} Coulomb

valley. By applying a high magnetic field we can reduce the size of the 0th Coulomb valley such that it doesn't allow for even a single additional charge state in the gap, thus confirming that the first Coulomb peaks in the electron and hole sides correspond to the addition of the *first* electron and *first* hole to the QD.

To analyze this quantitatively, we determine all the parameters of the QD directly from non-linear transport data, similar to those in fig. 2a. Specifically, the charging energies and level spacings between particle-in-a-box longitudinal modes for the first electron and first hole are $U_e = 19$ meV, $U_h = 25$ meV and $\Delta_e = 8$ meV, $\Delta_h = 11$ meV (see more details below). We estimate the band gap at 6 Tesla by subtracting the average charging energy and average level spacing for electrons and holes from the 0th Coulomb valley (55 meV), and obtain $E_{gap} = 24 \pm 2$meV at 6 Tesla. At the highest field in our measurements (9 Tesla) the size of the energy gap is smaller than the charging energies of either the electron or the hole dot, excluding the possibility of hidden charge states inside the 0th Coulomb valley.

2. Effects of higher particle-in-a-box longitudinal modes

The one-electron and one-hole excitation spectra presented in this paper correspond to the lowest quantized longitudinal mode. Quantized states of other longitudinal modes do not appear in the data presented in Figure 2 and Figure 4 because of their higher energy. We verified this by measuring excitation spectra at source drain voltages larger than in Figure 2a, and identifying longitudinal modes by their dependence on the length of the quantum dot. The level spacing extracted for a dot that is extended over both right and left gate electrodes is ~4 meV, and it increases continuously to >8 meV as the dot becomes localized either above the right or above the left gate electrode (using appropriate gate voltages). The latter corresponds to a confinement length smaller then 200 nm and is consistent with the lithographic dimensions given in Figure 1c. Therefore, higher longitudinal modes were ignored in the discussion of the one-electron and one-hole quantum dot.

The situation is different for the top two Coulomb peaks presented in Figure 3a, which involve three and four electrons in the quantum dot. Because of the increased size of the quantum dot at those charge states, the level spacing is reduced and higher modes

become occupied already at ~200 mT. At $B_{\|}$>200 mT it is favorable for all electrons to orbit in counterclockwise direction, thereby aligning their orbital magnetic moments parallel to the external magnetic field. This explains why the 3e and 4e addition spectra shown in Fig. 3a deviate for $B_{\|}$>200 mT from the 3rd and 4th excitations of the one-electron QD.

3. Comparison between the QD above the left and right gate electrodes

The ability to localize the QD on two physically different segments of the same nanotube (Figure S1) helps us determine whether the excitations observed at low energies depend on local properties in the nanotube such as localized disorder or specific properties of the source or drain electrodes. Figure S1c shows the non-linear conductance measured for a QD localized above the right gate electrode. The measurement is at finite magnetic field ($B_{\|}$=300 mT) allowing to resolve the four quantum states in the dot. The individual states are visible at negative bias and are absent at positive bias, indicating that the coupling of the QD to the source is much weaker than to the drain, as expected from its location. Accordingly, the capacitance between the QD and the source is smaller than the capacitance between the QD and the drain (C_s = 1/1.8 C_d, extracted from the slopes of the resonances in panel c). The energies of the quantum states in the dot extracted from this measurement are 0, 0.40, 0.98 and 1.33 meV (±5%). Figure S1d shows a similar measurement for a QD localized above the left gate electrode. As expected, here the tunnel coupling to the drain is weaker than that to the source, and hence the quantum states are probed by tunneling-in from the drain electrode (i.e. resonances appear at V_{sd}>0). The capacitance ratio (C_s = 2.2 C_d) is reversed compared to that in panel c. Most importantly, the excitations in panel c and d have identical energies up to an experimental uncertainty of ±5%. Similar measurements at other magnetic fields have also shown that the QD excitation energies do not depend on whether it is localized above the right or left gate electrode, demonstrating that the observed excitations are an intrinsic property of the nanotube.

4. Spin-orbit coupling vs. K-K' scattering

The four-fold degeneracy in NTs can be broken by extrinsic sources such as disorder, or by the intrinsic spin-orbit coupling. Disorder breaks the orbital symmetry of NTs in a trivial way and leaves doubly-degenerate spin states as in any other confined system with low symmetry. Spin-orbit coupling, on the other hand, breaks the degeneracy by coupling the orbital and spin degrees of freedom in parallel or anti-parallel configurations. Figure S2 shows how the theoretical four-fold energy spectrum for a single electron (Fig. 1b) changes in the presence of disorder (Fig. S2a) or spin-orbit coupling (Fig. S2b). In both cases the spectrum is split at $B_{\|} = 0$ into two Kramer doublets, but the nature of the new eigenstates is entirely different. In the case of disorder, the splitting results from mixing wavefunctions which revolve in opposite directions around the NT circumference, and hence the new eigenstates lack a definite sense of rotation around the circumference. Orbital angular momentum ceases to be a good quantum number for these states as is apparent from the fact that they have no coupling to the field ($dE/dB_{\|} = 0$ at zero field, ignoring the spin Zeeman coupling). In the presence of spin-orbit coupling, the components of angular momentum and spin parallel to the NT axis remain good quantum numbers. This is readily seen from the fact that the slopes in magnetic field, $dE/dB_{\|}$, remain finite even at zero magnetic field. SO interactions thus create non-trivial states in which the spin and orbital degrees of freedom are tied together.

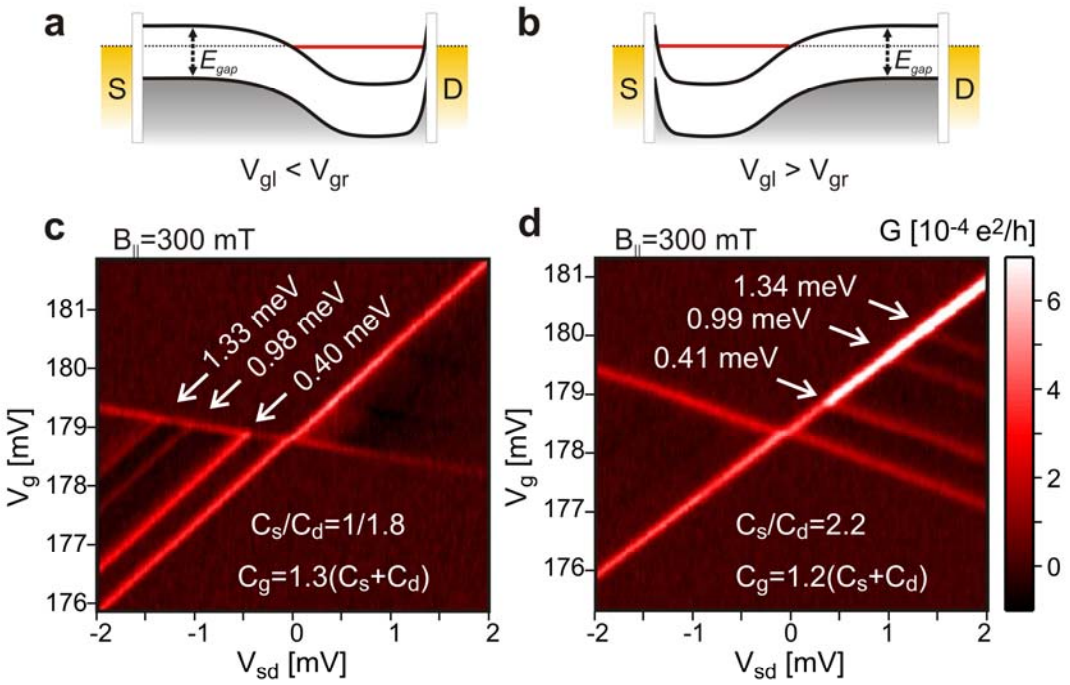

Figure S1: Independence of the one-electron excitation energies on the QD location. (a) Schematic band diagram for a one-electron QD formed above the right gate electrode. Here the longer barrier on the left side leads to a weaker tunnel coupling to the source electrode. (b) Same for a QD formed above the left gate electrode (c) Differential conductance, $G = dI / dV_{sd}$, measured as function of gate voltage, V_g, and source-drain bias, V_{sd}, at $B_{||} = 300$ mT for the transition from zero to one electron for a dot localized above the right gate electrode. The energies of the one-electron excitations that appear at negative V_{sd} are labeled. Also shown are the ratios of the capacitances between the QD and source (C_s), drain (C_d) and gate (C_g) electrodes, extracted from the slopes of the resonances. (d) Same for a QD localized above the left gate electrode.

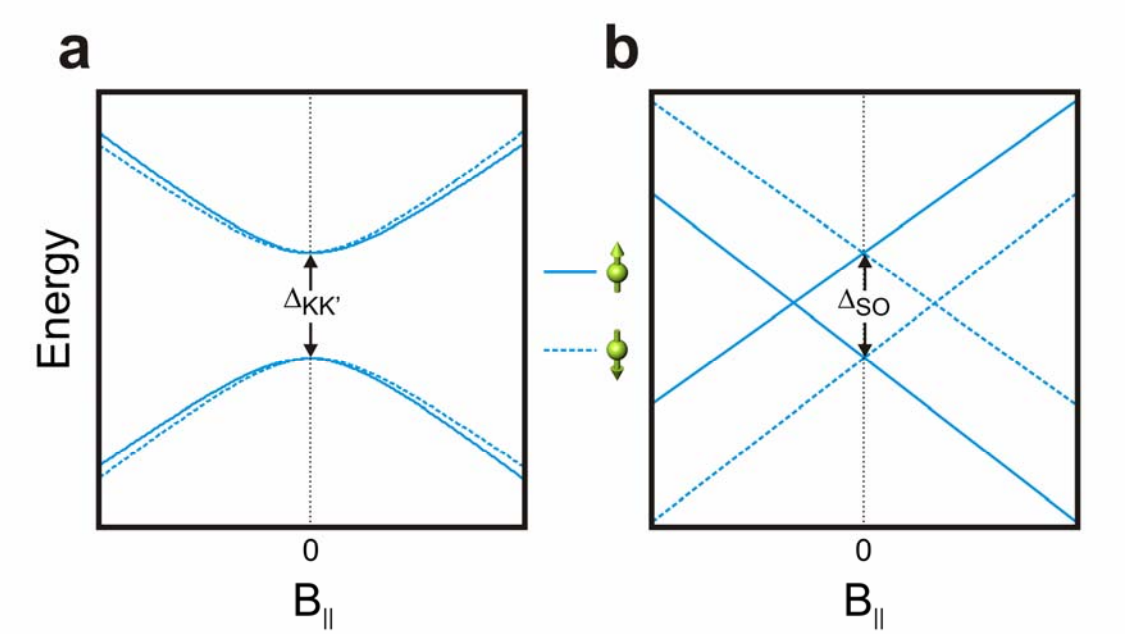

Figure S2: Breaking of four-fold degeneracy: spin-orbit coupling vs. KK' scattering. (a) The calculated one-electron spectrum as a function of parallel magnetic field in the presence of disorder-induced K-K' scattering and the absence of spin-orbit coupling. Dashed and solid lines correspond to spin moment down and up. (b) Same, but with spin-orbit coupling and without disorder-induced K-K' scattering.